Characterisation of micro turbine generator as a range extender using an automotive drive cycle for series hybrid electric vehicle application

Bin Raja Ahsan Shah, R. M., McGordon, A., Rahman, M. M., Amor-Segan, M. & Jennings, P.

DOI 10.1016/j.applthermaleng.2020.116302
ISSN 1359-4311

Publisher: Elsevier

Characterisation of micro turbine generator as a range extender using an automotive drive cycle for series hybrid electric vehicle application

Raja Mazuir Raja Ahsan Shah[1]*, Andrew McGordon[2], Md Mostafizur Rahman[1], Mark Amor-Segan[2], Paul Jennings[2]

[1] School of Mechanical, Aerospace and Automotive, Coventry University, Coventry, CV1 2JH, United Kingdom
[2] Warwick Manufacturing Group, Warwick University, Coventry, CV4 7AL, United Kingdom
* Correspondence: ac9217@coventry.ac.uk;

Abstract: This study investigated a micro turbine generator (MTG) as a range extender for a series hybrid electric vehicle application for a range of constant and dynamic power demand strategies. The power demands were calculated through a mathematical model based on a specific vehicle platform using the New European Drive Cycle (NEDC). The power demands were then used to characterize the MTG in a controlled test environment. Each of the strategies produced interesting results in terms of fuel consumption, specific emissions, net efficiency, and power responses. The experimental results revealed the lowest specific emissions, and fuel consumption while the MTG operated at constant power demand. One of the dynamic power demand strategies also produced low fuel consumption, but with higher specific emissions. Although exhaust emissions in each strategy were well below the Euro 6c limits. These results indicate the potential of MTG as a range extender in a series hybrid vehicle. Even, the MTG can be operated dynamically with relatively low fuel consumption and very low specific emissions, compared to the traditional approach of a constant power demand.

Keywords: Hybrid vehicle, Micro gas turbine, Energy storage, Validation, Propulsion system

1. Introduction

The electrification of passenger vehicles has meant a change to the vehicle market in recent years. From a report published by the International Energy Agency [1], the forecast sales of Electric Vehicles (EVs) in the year 2030 can reach 245 million due to the new environmental policies. The intense research in this area is influenced by the requirements of much stricter emissions legislation and reduction in fuel consumption [2]. For instance, the United Kingdom (UK) government is controlling fossil fuel vehicles in major cities by 2021 [4]. A report produced by the Society of Motor Manufacturers and Traders, UK [5] shows several vehicle electrification architectures have been commercially released in recent years such as full EVs and Hybrid Electric Vehicles (HEVs) with a combination of different powertrain technologies such as Jaguar E Pace and Volkswagen ID family. Research in the motorsports electrification has also become an important agenda in recent years such as Formula E and other motorsports events [6]. Several studies indicate that there has been considerable research on lithium-ion batteries as the energy storage medium of choice, but the traditional internal combustion (IC) engine will still dominate the market as the prime mover solution until 2040 [7, 8]. A study by Kumar and Sehgal [9] shows that the fuel cells have long been considered a potential solution, however, practical application is limited. Despite momentous progress in EVs technology in recent years, the limited driving range remained a crucial shortcoming to their wider popularity and acceptance.

Range extender is considered as an attractive alternative to prolong the driving range of EVs. A micro turbine generator (MTG) based range extender has several advantages over conventional IC engine range extender. It is has a high power density, a clean combustion process, and is reliable [10]. Besides, LDor et al. [11] explain that most architectures of the MTG combustion system allow for

multi-fuel capability with no hardware or software change required. The efficiency of MTG can be as good as traditional IC engine range extender with optimal design and careful selection of recuperator [12]. A recent study suggests that the thermal efficiency of MTG can reach 35% with recuperator effectiveness 0.7, pressure ratio 3.2, and turbine inlet temperature 1152K [13]. The studies by Karvountzis-Kontakiotis et al. [14] also found the influence of vehicle mass and ambient temperature on the performance of MGT as a range extender. Although substantial progress has been made in integrating MGT as a range extender for EVs, the relatively slow transient response of MGT remained a key challenge to the technology readiness level (TRL) for commercialization. However, the emissions benefit of MTG can outweigh some of its demerits, given that the increasingly stringent emissions standards are a new reality for both current and future generation automobiles. Cameretti et al. [15] also reported several emission reduction strategies from micro gas turbine while operating with low-grade fuels.

This paper focuses on the ability of the MTG to operate in the HEV based on four different strategies from a constant power level to operating more dynamic, for example setting power levels for a micro-drive cycle. The research aim is to run the MTG based on the New European Drive Cycle (NEDC) with several power demand strategies due to its power demand behaviours. The NEDC was chosen as a compromise between conflicting requirements. Although the NEDC has been superseded by the World Harmonized Light Vehicle Test Procedure (WLTP) for vehicle certification processes, this is a highly dynamic cycle and would not allow the MTG to operate in steady-state. The NEDC has some constant power requirements periods which are important to understand the post-dynamic response of an MTG. There are two drive cycles in the NEDC, namely Urban Drive Cycle (UDC) and Extra Urban Drive Cycle (EUDC). The UDC has three micro-cycles and all of the micro-cycles are repeated four times with a maximum speed of 50 km/h. The total duration of UDC is 780 seconds. On the other hand, the EUDC has only one micro-cycle and is not repeated with a maximum speed of 120 km/h and a total duration of 400 seconds. The aim is to be charge sustaining, so that these strategies could be used in an HEV, or a range extender HEV in a charge sustaining mode. This drive cycle shows an idealized speed-time profile and so is ideal for this type of study. This study approach delivers insights on several aspects of the MTG such as:

- Fuel consumption and emissions comparison for each power demand strategy
- Identify the overall best power demand strategy for the drive cycle studied.

A mathematical model and experimental methods are combined to characterize the MTG. In the following sections, the methods and the results will be discussed and explained in detail

2. MTG configuration

A typical MTG configuration consists of a single-stage turbine and a compressor connected by a shaft as shown in Figure 1. From the work performed by Costamagna et al. [16], it indicates that the shaft normally rotates above 100,000 revolutions per minute (rpm) and operates in a high-temperature environment. For these reasons, Belforte et al. [17] recommend using air bearings that can work well in both conditions. A three-phase alternating current (AC) generator is also connected to the turbomachinery via a shaft that acts as a rotor. Air is induced through the generator before it is compressed by the compressor. To protect the MTG from dust particles and to improve the air quality for performance, Shah et al. [18] use an air filter packaged at the front of the generator housing. The compressed air flows into a heat exchanger (recuperator) and increases the temperature of compressed air. Kolanowski [19] and Cavalca et al. [20] explain that the use of a recuperator can increase the performance efficiency by 10-15%. The compressed air enters a combustion chamber, where a fuel is injected continuously and the mixture ignited. The high-temperature gas from the combustion process turns the turbine and exits through the recuperator system into an exhaust system.

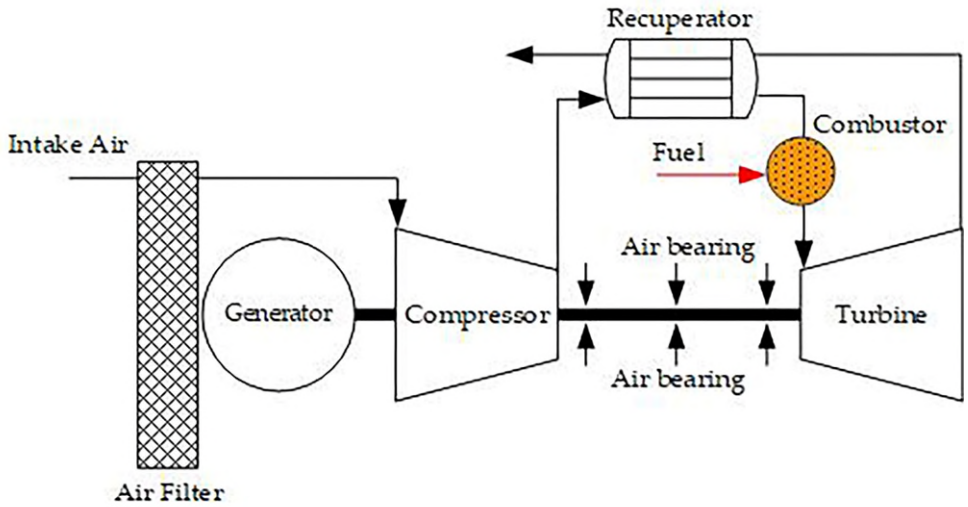

Figure 1. Basic architecture of the MTG for single-stage turbomachinery and coupled with a generator set with an air intake system

The research performed by Sarradj et al. [21] demonstrates that the MTG is most efficient when operating at a maximum power output. This characteristic limits the ability of the MTG to operate at different power levels with optimum fuel efficiency. Also, Dixit et al. [22] and Crombeen et al. [23] raise a concern for the implementation of the constant maximum power output of the propulsion system in terms of noise pollution. For instance, when the vehicle is at idle state, the MTG runs at maximum speed and may create an uncomfortable level of engine bay noise. Furthermore, Vora et al. [24] highlight the issue with the high exhaust flow rate and the temperature from the tail-pipe to pedestrian safety. Beer et al. [25] and Dhand et al. [26] have introduced an engine stop-start strategy that can feasibly minimize the tail-pipe temperature. However, this feature is traditionally difficult to achieve due to the response behaviours of the MTG for the start and shut-down modes as well as to meet the instantaneous power demands; these can easily be provided by the IC engine in contrast.

3. Mathematical model to identify power requirement for vehicle system

3.1. Generation of MTG Strategies

To analyze the vehicle energy requirement, the study is focused on four Power Demand Strategies (PDSs) that have the potential to be implemented on the MTG as listed in Table 1.

Table 1. Power demand strategies for the MTG in NEDC.

PDS	Definitions	Maximum power (kW)
1	Constant demand (average of the vehicle power demand requirement)	6.5
2	Speed dependent demand (based on 3 vehicle speed limits)	21.3
3	Micro-cycle demand (average power demand for each micro-cycle)	15.2
4	Power Ffollowing demand (instantaneous power demand)	25.0

It is assumed that the battery pack has reached a minimum State of Charge (SOC) and that the vehicle needs to meet the drive cycle in a range extender mode. The net energy at the end of NEDC is targeted to be zero, i.e. charge sustaining. This is to ensure that the battery pack size is optimized for cost, weight, and packaging. The PDS 1 uses the traditional method of operating the MTG which is to select an average power demand and run the MTG at this level continuously. The PDS 2 sets three power levels which are dependent on an average vehicle speed for a pre-determined time. The PDS 3 generates a power level based on the average power demand of a micro-cycle. The micro-cycle

in this case is considered to be any driving two consecutive stationary conditions. The PDS 4 uses the instantaneous power demand of the vehicle. All PDS profiles are shown in Figure 2. An executive saloon passenger vehicle has been used to generate the specific power and energy requirements used in this research; the vehicle specifications are given in Table 2. No regenerative braking is considered for this work to see the maximum energy can be derived from the MTG.

Table 2. Executive saloon passenger series hybrid vehicle specifications

Vehicle parameters	Value
Vehicle mass (kg)	2000
Drag coefficient	0.32
Frontal area (m^2)	2.05
Air density at 20 °C, 1 bar atm (kg/m^3)	1.2
Tyre rolling resistance	0.01
Average differential efficiency, η_{diff} (%)	98
Average motor efficiency, η_{mot} (%)	80
Average battery efficiency, η_{bat} (%)	95

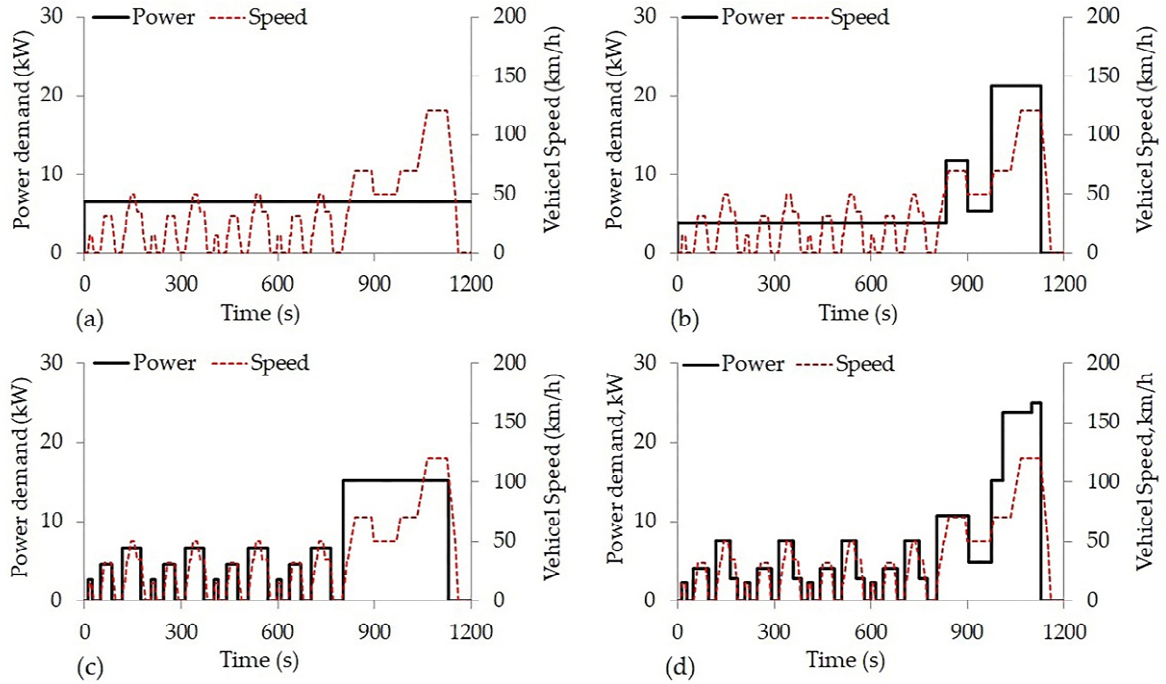

Figure 2. MTG power demands characteristics with four PDSs to meet the minimum battery SOC at NEDC: (a) PDS 1 (b) PDS 2 (c) PDS 3 (d) PDS 4. UDC runs from 0 seconds to 780 seconds and EUDC runs from 780 seconds to 1180 seconds

3.2. Power demand and energy demand requirements

Using the four PDSs, the vehicle model was simulated using a simple road load model to identify the energy output of the MTG and the vehicle available energy at the end of NEDC. The vehicle power demand can be expressed as:

$$P_{vd} = \int_{t_n}^{t_{n+1}} \left(F_{aero} + F_{rr} + ma + mg\sin\theta\right) v \, dt, \quad (1)$$

Where the denotes in the equation above are the vehicle's aerodynamics resistance, rolling resistance, acceleration resistance, gradeability resistance, and instantaneous velocity respectively. The

aerodynamics resistance is given by below where "ϱ" is the air density, "Cd" is the coefficient of drag, "A" is the vehicle frontal surface area and "v" is the velocity at a specific time.

$$F_{aero} = 0.5\varrho C_d A V_n^2, \quad (2)$$

And the vehicle rolling resistance is:

$$F_{rr} = mgC_{rr}, \quad (3)$$

"m" is the vehicle mass, "g" is the gravitational acceleration and "C_{rr}" is the tire rolling coefficient. For NEDC, the test is performed on a flat surface and therefore the gradeability resistance can be neglected. The battery power demand is defined as:

$$P_{bd} = \int_{t_n}^{t_{n+1}} E_{vd}/(\eta_{bat}\eta_{dif}\eta_{mot})dt, \quad (4)$$

And the available energy is defined by:

$$E_a = E_{pds} - E_{bd}, \quad (5)$$

"E_{pds}" is the energy produced in the PDSs. The available energy is the battery energy required to meet the drive cycle in combination with the MTG. The positive value of available energy indicates that the vehicle is expected to be charge positive at the end of the drive cycle. From the method, the MTG could be run according to its defined operating conditions and the battery pack would meet the remaining vehicle demand. Based on the vehicle energy requirement, the PDSs energy profiles of the MTG were derived according to Table 1, as shown in Figure 3.

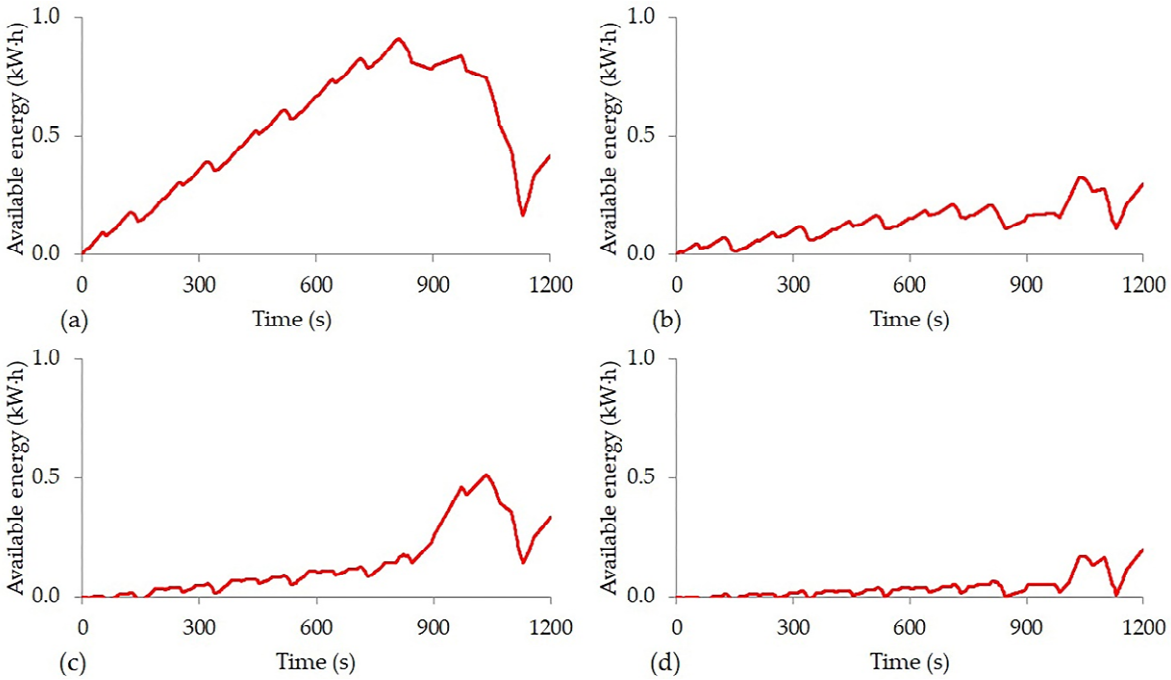

Figure 3. MTG available energy throughout NEDC using our PDSs: (a) PDS 1 (b) PDS 2 (c) PDS 3 (d) PDS 4

All PDSs can meet the minimum target batteries SOC at the end of the drive cycles. However, for the PDS 4, the MTG is not capable of meeting the fast responses of the power demand. Therefore the acceleration demand spikes are removed and the profile is smoothened to give a more achievable power demand profile. The initial MTG power output is set at zero for all PDSs. At the end of the NEDC, all of the PDSs have produced a similar amount of available energy (± 3 %). It can be observed that the PDS 2, 3 and 4 produce a low battery energy requirement across the drive cycles with a significant amount of battery energy storage required for the PDS 1. For these strategies, it is tempting

to consider the effect on battery pack size compared to the traditional method of operating the MTG, which is the PDS 1. For example, the battery in the PDS 2 is required to store a maximum of 0.33 kW·h per drive cycle, whereas the PDS 3 is only required to store 0.51 kW·h per drive cycle; 0.2 kW·h per drive cycle is required for PDS 4. Therefore, following the expected operation of the MTG at constant power output leads to the requirement of a larger pack than for the other more dynamic strategies.

The next step of the study was to deploy the PDSs into experimental tests on the MTG and to correlate them with the simulation results. In addition, the experimental test procedures allow a measurement of the specific fuel consumption (SFC), the emissions for the four PDSs over the drive cycle, and the MTG efficiency.

4. Experimental validation of the four power demand Strategies

A 25 kW electrical power output "black box" MTG with no access to the controller was used to generate the power output and the energy profiles based on the PDSs. To achieve this aim, the MTG was set-up in the test architecture as shown in Figure 4. The test architecture effectively mimics a series HEV or a range extender arrangement with the MTG, a battery load bank, and a battery measurement system. Several measurement sensors were used to measure all critical boundary parameters of the MTG such as inlet-outlet pressures and temperatures that influence the performance and the emissions of the MTG as shown in Table 3. The calibration of these sensors was performed based on the supplier's specifications and recommendations.

Table 3. Instrumentation probes and sensors for MTG experimental validation in automotive application.

Sensors	Measurement parameters	Specifications
Pressure Transducer	Pressure	35 kPA absolute pressure (-46 + 121 °C), Output: 0 to 5 Vdc ±0.03 Vdc, Linearity: 0.05% FSO, Compensated Temp Range: 16 to 71 °C
Resistance Temperature Detector	Temperature	Pt100 BS EN50751 Class A (-50 + 250 °C) 1/3 DIN
Thermo-couple	Temperature	K-Type (-200 to 1250 °C), Standard Limits of Error: > 2.2 °C or 0.75%

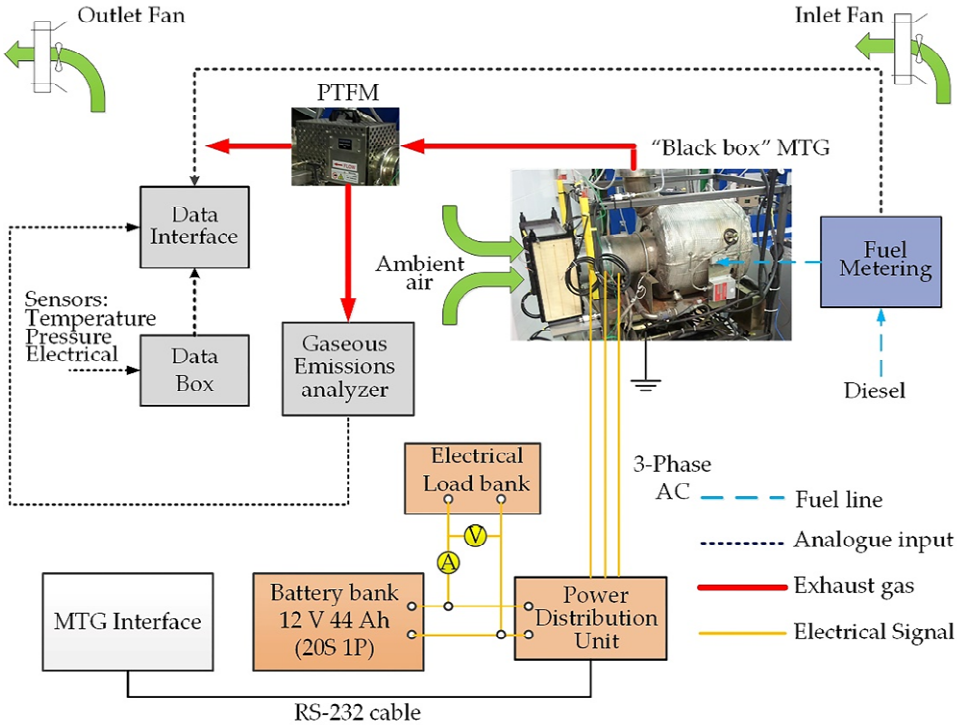

Figure 4. Test architecture of "black box" MTG using standard automotive air filtration system and equipment

Due to the limitation of the test cell facilities, the test procedure for all PDSs needs to be performed at ambient temperatures between 10 °C and 18 °C to maintain the steady power output and the net efficiency as suggested by Shah et al. [27]. Before the start of the test procedures, the inlet fan and the outlet fan were turned on until the test cell temperature reached the minimum working temperature and maintained at this value. It is also important to minimize the test cell pressure depression by controlling the speed of both fans. Each of the PDSs was controlled via the MTG interface. The initial condition of the power demand for all PDSs was set to zero at idle speed. The power demand is set to be ramped-up and ramped-down to the desired value within a one-second time-step based on the PDSs to emulate the typical drive cycle time step.

The MTG's Alternating Current (AC) generator unit was connected to power electronics that converted the AC power output to a direct current (DC) power output and in turn connected to a battery bank. The load bank was used to take the excess energy from the battery bank based on a predefined value of maximum battery SOC and a duty cycle. There were no gearing mechanism between the AC generator unit and the MTG. The speed of the alternator is regulated by the active front end by varying the frequency and voltage. When "motoring" (no combustion process) it behaves like a variable frequency drive. The net efficiency of the MTG at 18 °C ambient temperature is 25 %. The MTG was supplied with a calibrated diesel fuel through a temperature conditioned fuel meter. The diesel fuel properties are shown in Table 4.

Table 4. Calibrated diesel fuel properties (Carcal RF-06-08-B5)

Fuel properties	Value
Density at 15 °C (g/ml)	0.8348
Cetane number	52.3
Flash point (°C)	69
Viscosity at 40 °C (mm^2/s)	2.48
Polycyclic aromatic hydrocarbons (PCA) (% m/m)	5.5
Sulfur (mg/kg)	6.7
Carbon residue on 10% dist. residue (% mass)	< 0.1
Water content (mg/kg)	80
Fatty acid methyl ester content (% v/v)	4.7
Oxygen content (% m/m)	0.56
Carbon content (% m/m)	86.16
Hydrogen content (% m/m)	13.28
Gross calorific value (MJ/kg)	45.38
Net calorific value (MJ/kg)	42.56
C/H mass ratio	6.48
Atomic H/C ratio	1.8360
Atomic O/C ratio	0.0049

Within the exhaust system, the gaseous emissions without the after-treatment process were measured using a gas analyzer, which was connected to a pitot tube flow meter (PTFM). The calibration of the PTFM was based on work performed by Shah et al. [27]. Using the same parameters setting and test definitions, the experimental validation recurred two times. Average readings were used in the calculation of all output parameters below. The electrical power output was gained from the measured output voltage "V_o" and the output current, "I_o" using

$$P_o = V_o I_o, \quad (6)$$

The MTG efficiency was calculated using

$$\eta_{MTG} = P_o/(\dot{m}_f \,.\, Q_C), \quad (7)$$

Where "$\dot{m}_f$" is the fuel mass flow rate consumed by the MTG and "Q_c" is the fuel energy based on the fuel caloric value. The specific fuel consumption was obtained from

$$SFC = \dot{m}_f/P_o, \quad (8)$$

In terms of emissions, the Directive 70/220/EEC (Euro 6c) amended in 2004 was used as the baseline to measure the tail-pipe emissions of the MTG. For Diesel fuel, only Carbon Monoxide (CO), Nitrogen Oxide (NOx), and Hydro Carbon (HC) + NOx was considered in this work. Due to the nature of the MTG continuous combustion, the particulate matter measurement was neglected. The tail-pipe emission in g/km was calculated based on the total emission per cycle divided by the NEDC range per cycle.

5. Experimental validation results

5.1. MTG power demand responses

Figure 5 shows the power demand and the measured power output for all PDSs. For PDS 1, the power output response rate was 0.24 kW per every second demand from idle speed until the MTG can meet the power demand. This is probably due to the characteristics of the combustor that requires longer warm-up time until they can reach the optimum operating conditions such as combustion and recuperator temperatures as suggested by Gomes et al. [28]. The power output also exceeded the power demand by 12 % until the end of the cycle, potentially indicating some calibration error in the MTG software control system. A similar response is seen for PDS 2 during the initial ramp-up to 4 kW, and produced the same percentage of excess power output. However, the power response rate increased to 0.69 kW per every second demand when the power output was requested to be 12.5kW. When the power demand was reduced to 5 kW, the MTG responded similarly to the power ramp-up but required a longer duration to stabilize at this power level; approximately 0.1 kW per every second demand. From 5 kW to 20 kW, the power response rate was two times faster than the initial power ramp-up with 7 % excess power and maintained at this level. The MTG failed to achieve power demand when it was requested to idle from 20 kW within the time of the test, for more than 60 seconds.

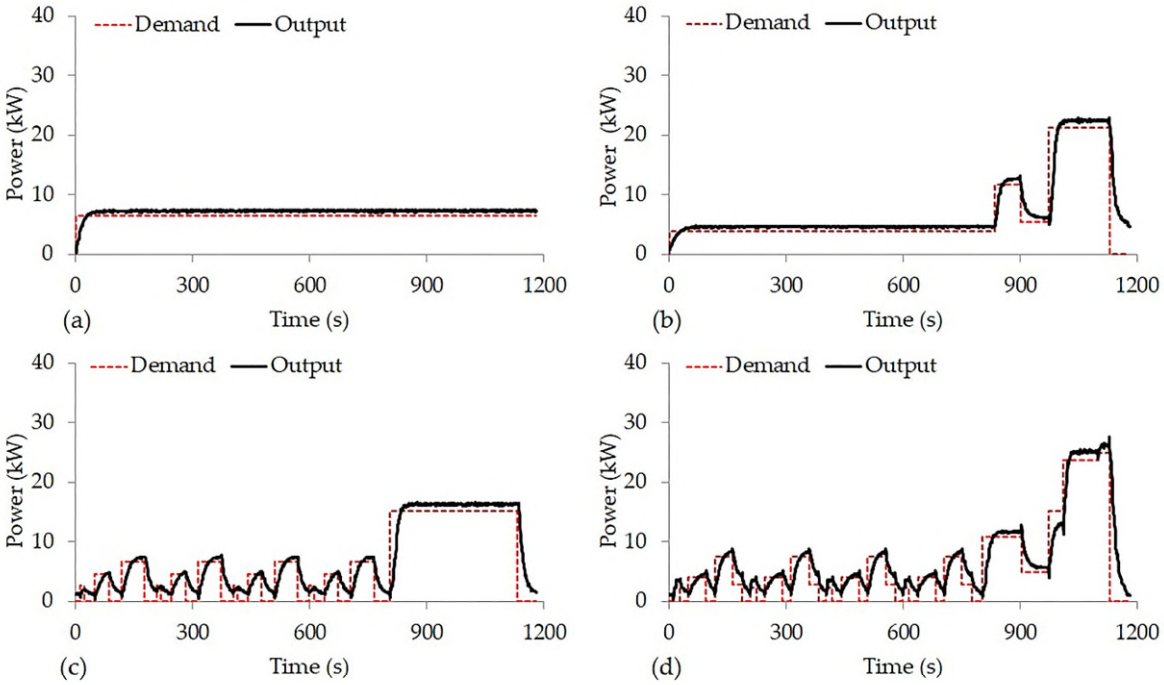

Figure 5. Analysis of the MTG at (a) PDS 1 (b) PDS 2 (c) PDS 3 and (d) PDS 4 vs. power outputs using NEDC

Different power output behaviours can be observed for the PDS 3 and the PDS 4 with more dynamic responses in the UDC. The power output was not able to settle down during ramp-up and ramp-down for both strategies. This was due to the short duration of the micro-cycles; the minimum power response rate was 0.25 kW per every second demand and the long time required for the MTG to respond to these demands changes. With the constant power demand in the EUDC of PDS 3, the MTG produced more stabilized power output with the delay still existed during ramp-up. However,

the dynamic demand in the EUDC of PDS 4 caused the MTG difficulties to achieve the higher power demand at a power response rate of 0.33 kW per every second demand.

5.2. Energy profiles

The energy profiles generated from these power demand strategies are shown in Figure 6. The PDS 1 produced a constant energy from the MTG. It can be seen that the MTG generated an excess of energy compared to the simulation predictions due to the 7 % higher energy output of the MTG for a given power demand setting. Figure 6 (a) shows that the energy generated by the MTG is more than that needed for propulsion for the UDC and therefore this excess energy needs to be stored in the battery. The vehicle was therefore in battery charging mode in this part of the drive cycle. In the EUDC, the vehicle power demand exceeded that power generated by the MTG, and energy was required to be taken from the battery to meet the propulsion needs.

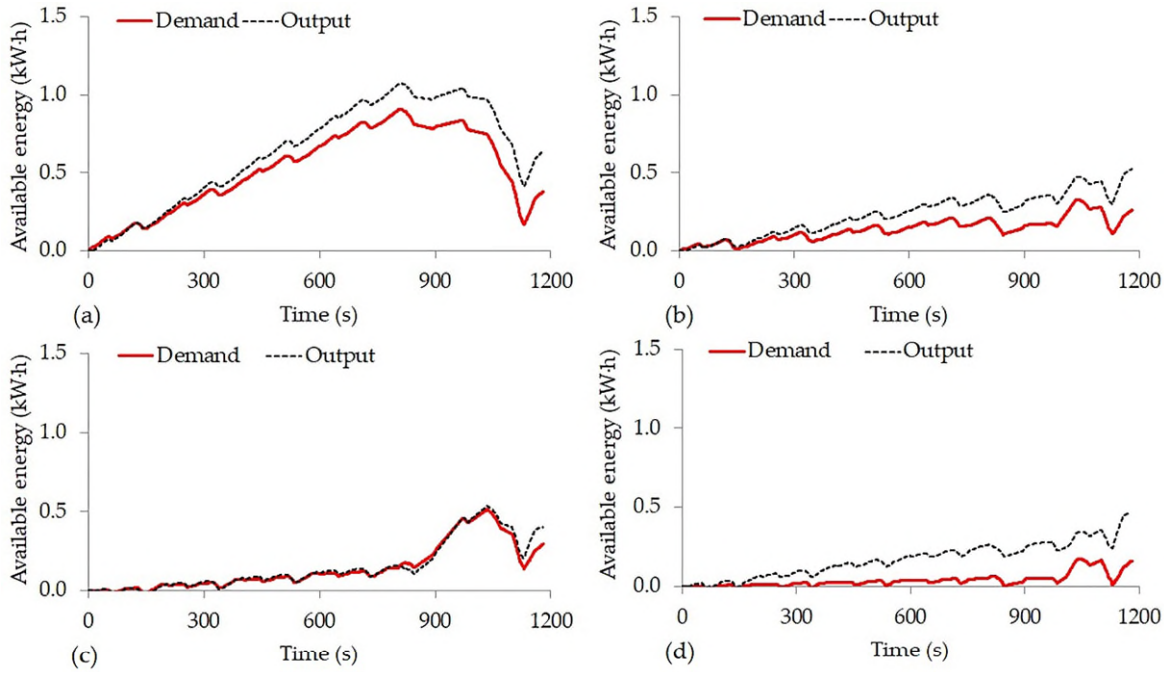

Figure 6. Analysis of MTG for energy behaviours between simulated energy availability and tested energy of four PDSs based on NEDC: (a) PDS 1 (b) PDS 2 (c) PDS 3 (d) PDS 4

Therefore, in the EUDC, the vehicle was in charge depleting mode. These modes are a function of the MTG control strategy and a result of operating at a single average power output for the whole drive cycle. Besides, the long response time of the MTG means that in the case of regenerative braking, the battery is required to absorb not only the braking power but that generated by the MTG also. This cycle will lead to a larger battery SOC swing than other strategies leading to a potential lower battery lifetimes compared to the other strategies if the battery sizes for all four PDSs are identical. Alternatively, PDS 1 requires a larger battery pack than for the other three PDSs as it shows the most available excess energy for the energy storage device.

In the PDS 2, the MTG produced smaller excess energy than for the PDS 1 in the UDC, reflected the lower power demand there. Since the MTG power demand in the EUDC was increased in line with the vehicle power demand, this part of the drive cycle was now in charged sustaining mode. Interestingly, although most of the time the MTG was unable to meet the dynamic demand in the

PDS 3, the MTG energy output showed the closest correlation with the simulation. In both UDC and EUDC, this strategy was slightly charged positive; i.e. the MTG was generating a slight excess of energy. The PDS 4 was the most dynamic MTG control strategy and therefore expected to show the best management of excess energy. Similar to the PDS 3 in the UDC, the MTG was not able to follow the power demands. In contrast to the PDS 3, it provided an excess of energy generated compared to the prediction. The excess energy generated showed similarities to that seen for PDS 2. It can, therefore, be recommended that to minimize the size of the battery pack for operating the MTG on a series HEV, a combination of strategies should be adopted. For the UDC, the PDS 3 showed the least amount of excess energy required to be absorbed by the battery. For the EUDC, either the PDS 3 or the PDS 4 should be used. However, the selection of the most appropriate strategy should also be based on the SFC and the emissions behaviour.

5.3. SFC, net efficiency and gaseous emissions

5.3.1. SFC

In terms of the SFC, the behaviour of all PDSs is broadly followed the same trend as the power output as shown in Figure 7 and the average value of SFC is shown in Table 5. This indicates that the SFC has a proportional relationship with the power output. The PDS 1 has a peak SFC during initial power demand. The peak SFC was influenced by the MTG behaviour during the initial ramp-up power demand, as more fuel was required until the power output can be stabilized. The difference between the UDC and the EUDC was 4 % with a total average SFC of 509 g/kW·h. This value is higher than the IC engine range extender with similar performance at a similar power demand as found in studies by Turner et al. [29] and Kulkarni et al. [30]. Similar behaviour can also be seen in the PDS 2 during the initial ramp-up. The MTG operated in constant SFC in the UDC but 28 % more than PDS 1. There was a slight improvement in the EUDC region. The combination of the steady-state and dynamic power demands in the PDS 2 has no significant advantages compared to the PDS 1. The lower average value in the EUDC can be potentially combined with PDS 1 for further SFC reduction. On the other hand, both of the PDS 3 and the PDS 4 have a high average SFC due to the dynamic low power demands in the UDC, particularly in the initial ramp-up of the PDS 2. The high power demand for both strategies in the EUDC consumed more fuel than PDS 1 and PDS 2 that suggested the strategies might not be the most suitable when fuel economy and emissions reduction is a priority.

Table 5. Average SFC for four PDSs in NEDC.

Power Strategies	UDC	EUDC	Total average
PDS 1 (g/kW·h)	516	494	509
PDS 2 (g/kW·h)	650	485	592
PDS 3 (g/kW·h)	935	555	802
PDS 4 (g/kW·h)	793	633	737

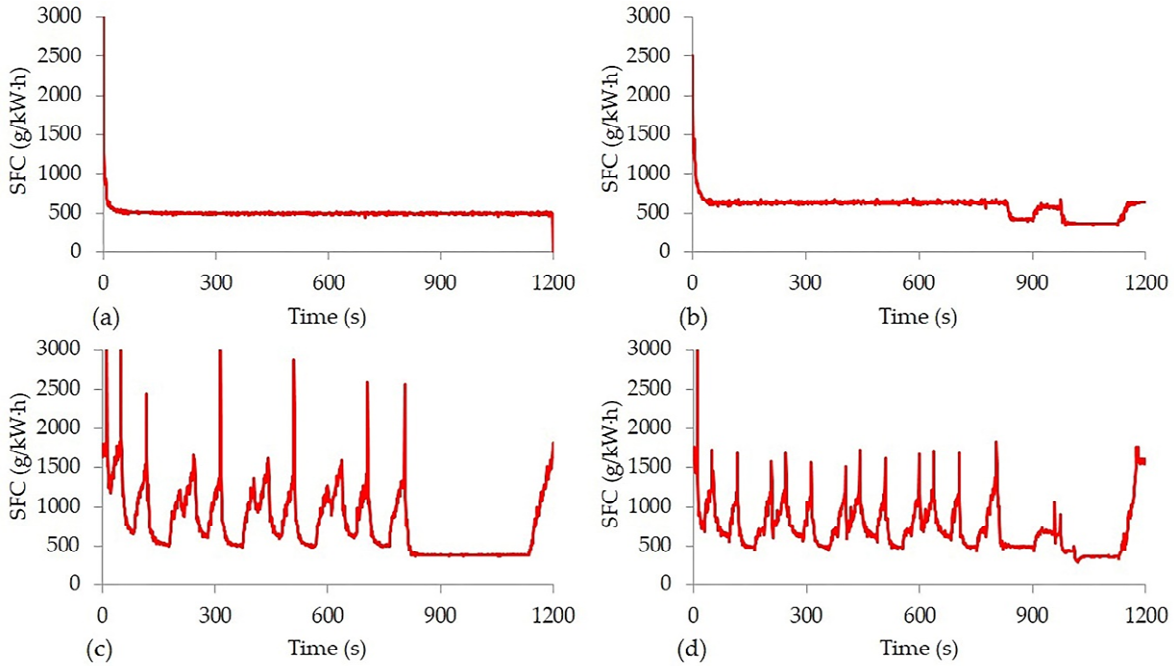

Figure 7. Analysis of MTG for fuel consumption behaviours of four PDSs based on NEDC: (a) PDS 1 (b) PDS 2 (c) PDS 3 (d) PDS 4

5.3.2. Net efficiency

The ratio of power output and energy of fuel is demonstrated in Figure 8. The MTG was operated at a total average of 17 % net efficiency for PDS 1 throughout the NEDC, which is much less than the maximum net efficiency that it can generate at 25 %.

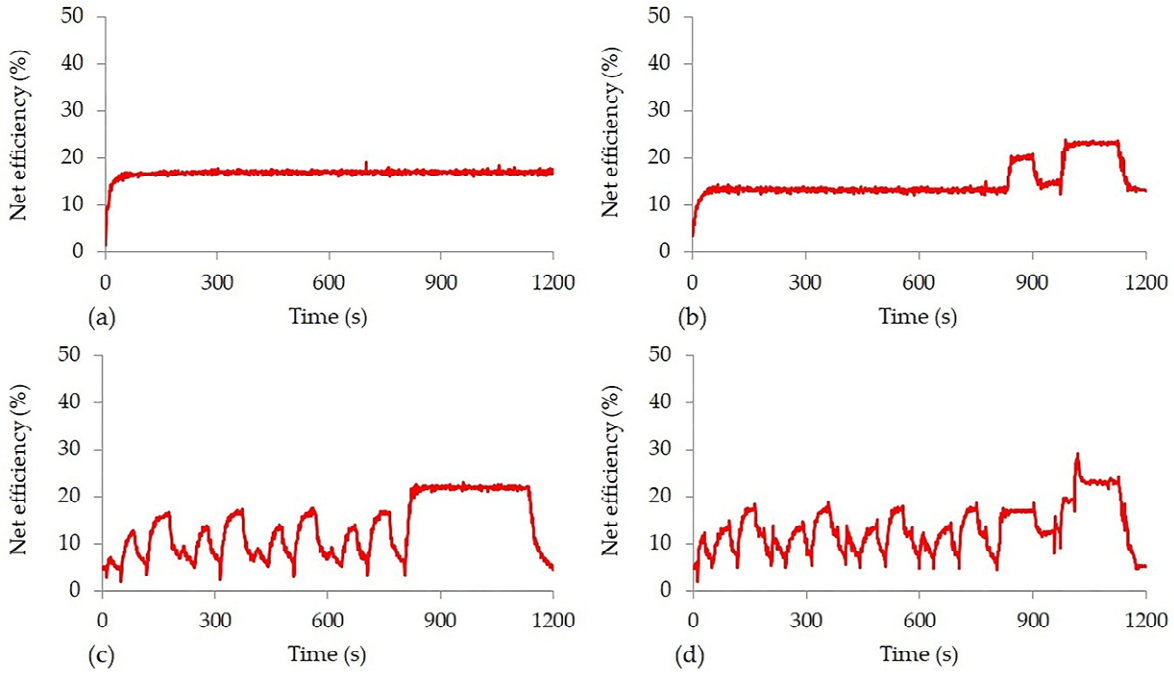

Figure 8. Analysis of MTG for net efficiency of four PDSs based on NEDC: (a) PDS 1 (b) PDS 2 (c) PDS 3 (d) PDS 4

The lower constant power demand in the UDC of the PDS 2 has a lower total net efficiency (15 %), which is almost half of the maximum net efficiency. This indicates that to operate the MTG at constant low power output can cause several issues such as thermal and noise pollutions. From Besides, Liu et.al [31] and Tang et al. [32] suggest that it is not economical to harvest the low-grade heat energy from. In the EUDC, the average net efficiency was higher with the peak value close to the maximum net efficiency of the MTG specification when operated at high power demand. Both PDS 3 and PDS 4 produced the same total average efficiency of 13 % with a slight advantage for PDS 3 in the EUDC and PDS 4 in the UDC due to the high constant power demand.

5.3.3. Gaseous emission

Figure 9 presents the variations in CO emissions for all four PDSs over the NEDC. CO emissions followed the power demand curve, and therefore the fuel consumption trend in each PDS.

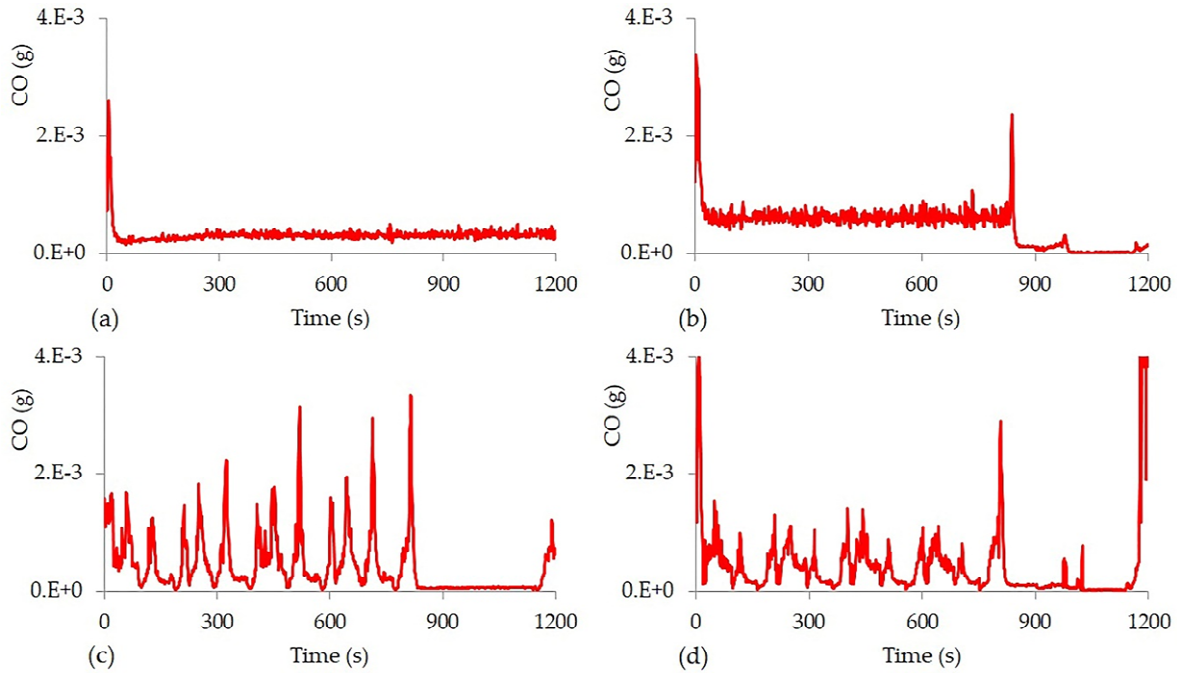

Figure 9. Analysis of MTG for CO emission behaviours of four PDSs based on NEDC: (a) PDS 1 (b) PDS 2 (c) PDS 3 (d) PDS 4

Constant power demand resulted in steady CO emissions (PDS 1 and PDS 2 in the UDC), where dynamic CO emissions for ramped-up and ramped-down power demand (PDS 3 and PDS 4). In addition, the MTG produced higher CO emissions in the UDC compared to the EUDC, except for PDS1. This may be related to the higher operating temperature of MTG in the EUDC mode compared to the UDC. The high temperature in the EUDC is due to higher operating speed and power. The reduction in CO emission from diesel combustion at higher temperatures is evident in the literature as well [33, 34]. For all PDSs, the highest peak in CO emissions occurred at the start-up phase of the MTG. This was likely due to a richer air-fuel ratio, and cold system, etc. The cumulative emissions factor over the entire NEDC cycle revealed the lowest CO emission (0.04 g/km) for PDS 1, where the other PDSs produced slightly higher CO emissions (0.05 g/km). NOx emissions also varied with the power demand and speed in each PDS.

As shown in Figure 10, peak NOx emissions from the EUDC was much higher than UDC except for PDS 1, which is again related to the operating speed and power, and therefore the operating temperature. However, NOx emissions remained steady in the UDC for PDS 1 and PDS 2, although operating speed varied but not the power demand. This suggests that NOx emissions rather depends more on power demand than operating speed. Increased NOx emissions at high operating temperatures are well established in diesel combustion literature [14, 35]. This behaviour shows that

it is important to run the MTG at a low power demand to minimize NOx emissions. The combination of HC + NOx emissions as shown in Figure 11 were dominated by NOx emissions, which suggests that there were very little unburnt hydrocarbons in the exhaust indicating a clean-burning process. However, during the initial power ramped-up from idle speed, the MTG generated higher HC and CO emissions probably due to the low operating temperature within the combustor system.

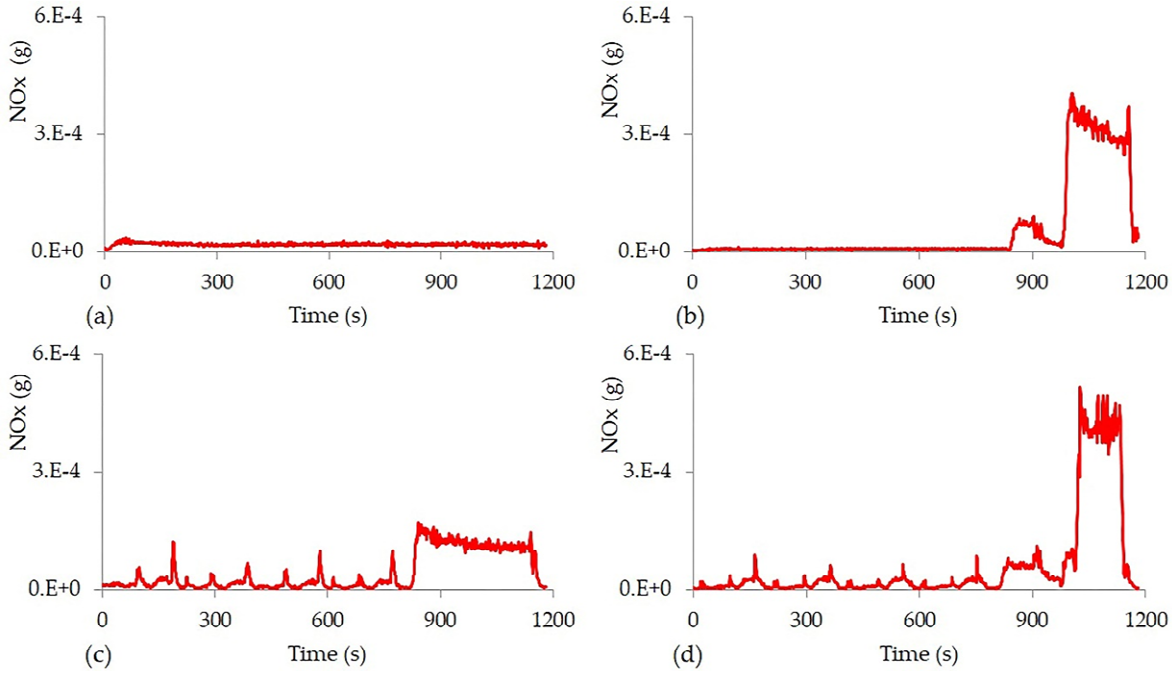

Figure 10. Analysis of MTG for NOx emission behaviours of four PDSs based on NEDC: (a) PDS 1 (b) PDS 2 (c) PDS 3 (d) PDS 4

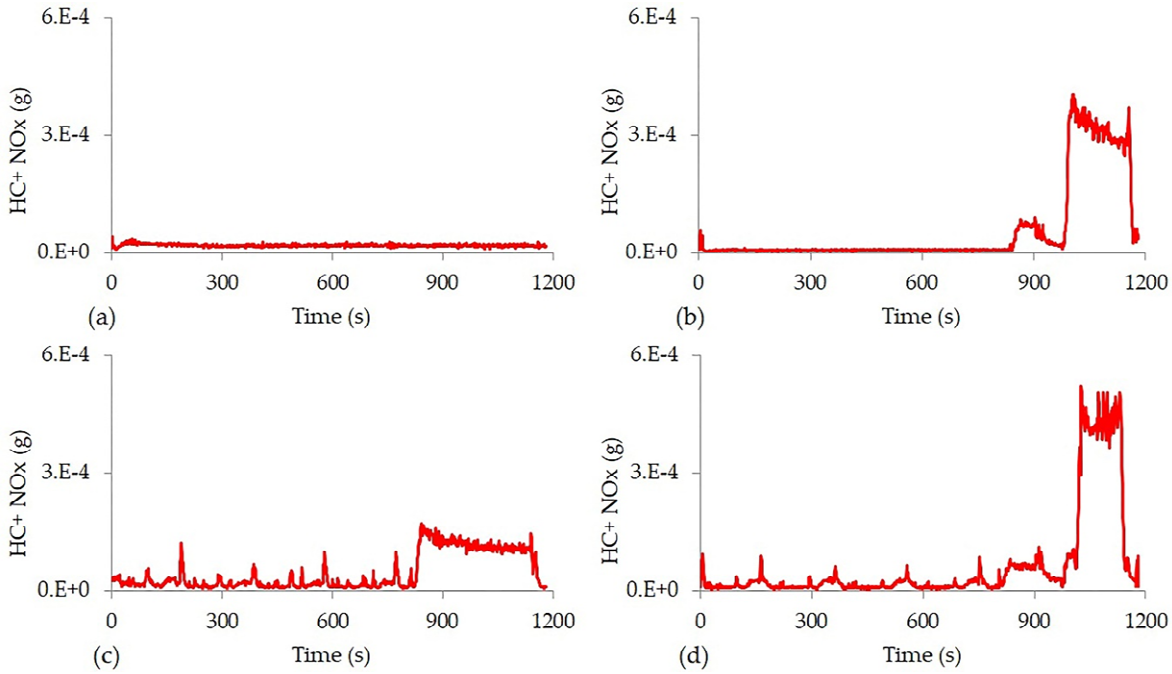

Figure 11. Analysis of MTG for HC + NOx emission behaviours of four PDSs based on NEDC: (a) PDS 1 (b) PDS 2 (c) PDS 3 (d) PDS 4

The cumulative NOx and NOx + HC emissions factor over the NEDC cycle revealed again the lowest NOx emissions from PDS 1 followed by PDS 3, PDS 2, and PDS 4 respectively. This again correlates quite well with the maximum power demand trend in the PDSs. Table 6 shows a summary of the average SFC and the average gaseous emissions for the vehicle over the NEDC; this allows for a comparison with the Euro 6c standards for passenger vehicles.

Table 6. Average SFC for four PDSs in NEDC.

Combined value	EURO 6c limit	PDS 1	PDS 2	PDS 3	PDS 4
SFC (g/kW·h)	N/A	508	592	802	737
CO (g/km)	0.5	0.04	0.05	0.05	0.05
NOx (g/km)	0.08	0.002	0.006	0.005	0.007
HC + NOx (g/km)	0.17	0.0022	0.0063	0.0051	0.0072

The PDS 1 resulted in the lowest fuel consumption, as well as CO, NOx, and HC emissions. CO emissions from other PDSs found 20 % higher than PDS 1, but remained well below the Euro 6 emissions limit. Similarly, for NOx emissions, all PDSs showed emissions well below the Euro 6 limit, with PDS 1 having the lowest overall emissions. In terms of HC + NOx emissions, the result is not significantly different compared to NOx emissions with the PDS 4 showing the highest value. All of PDSs results indicate that the raw emissions of the MTG require no exhaust after-treatment which potentially reduces the system cost and complexity.

6. Conclusions

The results reported in Section 4 can be used to provide information about the recommended strategy for the operation of an MTG. From the results, it is apparent that there will be compromises to operation depending on the dominant requirements of the application. From the SFC perspective, the PDS 1 shows the lowest value, and the PDS 3 having a much higher SFC value. The fuel consumption results of ~7.5 ℓ/100km are larger than that seen with the 3.0d Jaguar XJ, which achieves 5.9ℓ/100km over the NEDC, on which the simulation results were based. The average efficiency of an MTG is lower than the efficiency of a modern diesel IC engine and this is reflected in these figures. This indicates that the most promising future market for an MTG in automotive applications is in a range extender application where the IC engine runs for less duration than in a standard HEV.

For the application considered, i.e. a prime mover for a series HEV, since the gaseous emissions are more than ten times lower than the Euro 6c limits, less importance can be attached to these results when considering an overall preferred strategy. Unlike the IC engine, NOx emissions do not change significantly with changes in demand, therefore a dynamic strategy can be used rather than a continuous operating point normally seen for this MTG technology. It should be emphasized that the emissions described in this paper are raw MTG-out emissions and therefore no complex after-treatment is required to meet legislative targets. Future work in this area should verify the expected small amount of particulate matter in the MTG exhaust.

Specifying the battery from an energy perspective indicates that the PDS 3 is preferred to allow a smaller battery size than the other strategies. However, from Figure 6, the PDS 3 should be preferred for the urban part of the drive cycle, and the PDS 4 for the extra-urban part; this will allow an overall minimum battery size. The combination of these dynamic power strategies need further investigation due to the limitation of the MTG, particularly the PDS 3. The operation of the dynamic power demand could potentially have an impact on reliability. Besides, the behaviour of the power response under

dynamic power demand shows considerable delay compared to the IC engine behaviour. This behaviour can potentially be rectified with a control strategy that predicts future power delivery to meet the power demand at a specific time. In both PDSs, the MTG was not able to follow the power demand profiles for the ramped-up and ramped-down demands. This indicates that the MTG technology must be married with an energy buffer to allow operation in a vehicle. This also has implications for the power output requirements of the battery pack. The MTG considered, which has a maximum power demand of 25 kW, can provide the prime mover power to drive an executive saloon vehicle over the NEDC for all four strategies. This represents a considerable opportunity for the downsizing of the prime mover. However, further work is required before the MTG can be implemented in the automotive domain. This work is also valid for extrapolation to other prime movers with similarly poor dynamic performance, such as fuel cells. The dynamic operation of fuel cells is not widely done in practice but the adoption of the strategies described in this manuscript could offer the potential for downsizing the batteries in fuel cell electric vehicles.

Author Contributions: R.M.B.R.A Shah: Conceptualization, Methodology, Software, Validation, Formal analysis, Investigation, Resources, Writing - Original Draft, Writing - Review & Editing, Visualization, Project administration. **A. McGordon:** Conceptualization, Validation, Writing - Original Draft, Writing - Review & Editing, Supervision. **M.M. Rahman:** Validation, Formal analysis, Writing - Original Draft, Writing - Review & Editing. **M. Amor-Segan:** Conceptualization, Validation, Writing - Original Draft, Writing - Review & Editing, Supervision. **P. Jennings**: Conceptualization, Supervision, Project administration, Funding acquisition.

Funding: This research was funded by TECHNOLOGY STRATEGY BOARD, grant number 400224.

Acknowledgments: The authors would like to thank the technical partners, Jaguar Land Rover and Bladon Micro Turbine Limited for providing the technical supports, and Science City Energy Efficiency and Demand Project for the facilities. Finally, a special thanks to all Vehicle Energy Facility technicians at the University of Warwick for their commitments and ideas.

Conflicts of Interest: On behalf of all the authors, the corresponding author states that there is no conflict of interest.

References

1. IEA, Global EV Outlook 2020. Paris https://www.iea.org/reports/global-ev-outlook-2020; 2020 [accessed 01 May 2020].
2. Wappelhorst, S.; Mock, P.; Yang, Z. Using Vehicle Taxation Policy to Lower Transport Emissions: An Overview for Passenger Cars in Europe. The International Council On Clean Transportation. 2018.
3. ECE/TRANS/WP.29. In: UNECE, (ed.). UNECE. 2018.
4. Ultra Low Emission Zone. https://tfl.gov.uk/modes/driving/ultra-low-emission-zone; 2020 [accessed 07 April 2020].
5. SMMT Vehicle Data. https://www.smmt.co.uk/vehicle-data/; 2020 [accessed April 2020]
6. Chatzikomis, C.; Sorniotti, A.; Gruber, P.; Bastin, M.; Shah, R.M.; Orlov, Y. Torque-Vectoring Control for an Autonomous and Driverless Electric Racing Vehicle with Multiple Motors. SAE Int J Veh Dyn, Stab, and NVH. 2017; 1: pp. 338-351. https://doi.org/10.4271/2017-01-1597.
7. The Roadmap Report. Towards 2040: A Guide to Automotive Propulsion Technologies. Advanced Propulsion Centre UK. https://www.apcuk.co.uk/opportunities-for-you/roadmap-report/; 2015. [accessed 04 May 2020].
8. Eckerle, W.; Sujan, V.; Salemme, G. Future Challenges for Engine Manufacturers in View of Future Emissions Legislation. 2017; SAE Technical Paper 2017-01-1923. https://doi.org/10.4271/2017-01-1923.
9. Kumar, A.; Sehgal, M. Hydrogen Fuel Cell Technology for a Sustainable Future: A Review. 2018; SAE Technical Paper 2018-01-1307. https://doi.org/10.4271/2018-01-1307.
10. Cesare, D. M.; Cavina, N; Paiano, L. Technology Comparison for Spark Ignition Engines of New Generation. SAE Int J Engines 2017; 10: pp. 2513-2534. https://doi.org/10.4271/2017-24-0151

11. LdOR, M.A.R.D.N.; Santos, E.C.D.S.; Gomes, E.E.B.; Dias, F.L.G.; Velásques, E.I.G; Carrillo, R.A.M. Micro Gas Turbine Engine: A Review, Progress in Gas Turbine Performance. 2013; IntechOpen.
12. Xiao, G.; Yang, T.; Liu, H.; Ni, D.; Ferrari, M.L.; Li, M.; Luo, Z.; Cen, K.; Ni, M. Recuperators for micro gas turbines: A review. Applied Energy 2017; 197: pp. 83-99. https://doi.org/10.1016/j.apenergy.2017.03.095
13. Ji, F.; Zhang, X.; Du, F.; Ding, S.; Zhao, Y.; Xu, Z.; Wang, Y.; Zhou, Y. Experimental and numerical investigation on micro gas turbine as a range extender for electric vehicle. Applied Thermal Engineering 2020; 173: 115236. https://doi.org/10.1016/j.applthermaleng.2020.115236.
14. Karvountzis-Kontakiotis, A.; Andwari, A.M.; Pesyridis, A.; Russo, S.; Tuccillo, R.; Esfahanian, V. Application of micro gas turbine in range-extended electric vehicles. Energy 2018; 147: pp. 351-361. https://doi.org/10.1016/j.energy.2018.01.051
15. Cameretti, M.S.; Tuccillo, R. Combustion features of a bio-fuelled micro-gas turbine. Applied Thermal Engineering 2015; 89: pp. 280-290. https://doi.org/10.1016/j.applthermaleng.2015.05.057
16. Costamagna, P.; Magistri, L.; Massardo A.F. Design and part-load performance of a hybrid system based on a solid oxide fuel cell reactor and a micro gas turbine. Journal of Power Sources 2001; 96: pp. 352-368. https://doi.org/10.1016/S0378-7753(00)00668-6.
17. Belforte, G.; Colombo, F.; Raparelli, T.; Trivella, A.; Viktorov, V. High-speed electrospindle running on air bearings: Design and experimental verification. Meccanica 2008; 43: pp. 591-600. https://doi.org/10.1007/s11012-008-9135-5.
18. Shah, R.M.A.; McGordon, A.; Amor-Segan, M.; Jennings, P. Micro Gas Turbine Range Extender - Validation Techniques for Automotive Applications. IET Conference Proceedings 2013. https://digital-library.theiet.org/content/conferences/10.1049/cp.2013.1913.
19. Kolanowski, B.F. Guide to microturbines. New York, USA: The Fairmont Press, Inc. 2004.
20. Cavalca, D.F.; Bringhenti, C.; Tomita, J.T.; Silva, O.F.R. Microturbine Design Point Evaluation and Optimization Considering Pollutant Emissions and Thermoeconomic Approach. Journal of Propulsion and Power 2015; 31: pp. 1107-1116. https://doi.org/10.2514/1.B35511.
21. Sarradj, E.; Geyer, T.; Jobusch, C.; Kießling, S.; Neefe, A. Noise Characteristics of a Micro Gas Turbine for Use in a Serial Hybrid Concept. 2014; SAE Technical Paper 2014-01-2066. https://doi.org/10.4271/2014-01-2066.
22. Dixit, M.; Sundaram, V.; Kumar S, S. Optimization of Muffler Acoustics Performance using DFSS Approach 2016; SAE Technical Paper 2016-01-1292, https://doi.org/10.4271/2016-01-1292.
23. Crombeen, P. Advanced Car Specialties Ltd. Exhaust gas muffler. U.S. Patent Application 2005; 11/017,132.
24. Vora, K.; Patil, A.; Halbe, V. A Systems Approach to Automotive Exhaust System Development. 2003; SAE Technical Paper 2003-26-0029, https://doi.org/10.4271/2003-26-0029.
25. Beer, J.; Teulings, W. Optimized Start Strategy for Stop/Start Operation of a μ-Hybrid Vehicle. 2007; SAE Technical Paper 2007-01-0298, 2007, https://doi.org/10.4271/2007-01-0298.
26. Dhand, A.; Cho, B.; Walker, A.; Kok, D.; Burgess, M.; Semar, B. Optimization potential of the vehicle launch performance for start–stop micro-hybrid vehicles. Proceedings of The Institution of Mechanical Engineers Part D-Journal of Automobile Engineering – Proc Inst Mech Eng D-J Auto 2010; 224: pp. 1059-1070. https://doi.org/10.1243/09544070JAUTO1496.
27. Shah, R. M. B. R. A.; Al Qubeissi, M.; McGordon, A.; Amor-Segan, M.; Jennings, P. Micro Gas Turbine Range Extender Performance Analysis Using Varying Intake Temperature. Automotive Innovation. (In-Press)
28. Gomes, E.E.B.; Do Nascimento, M.A.R.; Lora, E.E.S.; Pilidis, P.; Haslam, A. (2004). Performance evaluation and case studies of microturbines fuelled with natural gas and diesel. Proceedings of the Institution of Mechanical Engineers, Part A: Journal of Power and Energy 2004; 218(8): pp. 599-607. https://doi.org/10.1243/0957650042584276.
29. Turner, M.; Turner, J.; Vorraro, G. Mass Benefit Analysis of 4-Stroke and Wankel Range Extenders in an Electric Vehicle over a Defined Drive Cycle with Respect to Vehicle Range and Fuel Consumption. 2019; SAE Technical Paper 2019-01-1282. https://doi.org/10.4271/2019-01-1282
30. Kulkarni, D.P.; Vajjha, R.S.; Das, D.K.; Oliva, D. Application of aluminum oxide nanofluids in diesel electric generator as jacket water coolant. Applied Thermal Engineering 2008; 28: pp. 1774-1781. https://doi.org/10.1016/j.applthermaleng.2007.11.017.

31. Liu, X.; Deng, Y.D.; Chen, S.; Wang, W.S.; Xu, Y.; Su, C.Q. A case study on compatibility of automotive exhaust thermoelectric generation system, catalytic converter and muffler, Case Studies in Thermal Engineering 2014; 2: pp 62-66. https://doi.org/10.1016/j.csite.2014.01.002.
32. Tang, Z.B.; Deng, Y.D.; Su, C.Q.; Shuai, W.W.; Xie, C.J. A research on thermoelectric generator's electrical performance under temperature mismatch conditions for automotive waste heat recovery system, Case Studies in Thermal Engineering 2015; 5: pp. 143-150. https://doi.org/10.1016/j.csite.2015.03.006.
33. Chiaramonti, D.; Rizzo, A.M.; Spadi, A.; Prussi, M.; Riccio, G.; Martelli, F. Exhaust emissions from liquid fuel micro gas turbine fed with diesel oil, biodiesel and vegetable oil. Applied Energy 2013; 101: pp. 349-356. https://doi.org/10.1243/095765004258427.
34. Saifuddin, N.; Refal, H.; Kumaran, P. Performance and emission characteristics of micro gas turbine engine fuelled with bioethanol-diesel-biodiesel blends. International Journal of Automotive & Mechanical Engineering 2017; 14(1). https://doi.org/10.15282/ijame.14.1.2017.16.0326.
35. Karvountzis-Kontakiotis, A.; Andwari, A.M.; Pesyridis, A.; Russo, S.; Tuccillo, R.; Esfahanian, V. Application of micro gas turbine in range-extended electric vehicles. Energy 2018; 147: pp. 351-361. https://doi.org/10.1016/j.energy.2018.01.051